Anti-Extra Domain B Splice Variant of Fibronectin Antibody–Drug Conjugate Eliminates Tumors with Enhanced Efficacy When Combined with Checkpoint Blockade

Andrea T. Hooper[1], Kimberly Marquette[2], Chao-Pei Betty Chang[1], Jonathon Golas[1], Sadhana Jain[2], My-Hanh Lam[1], Magali Guffroy[3], Mauricio Leal[2], Hadi Falahatpisheh[3], Divya Mathur[1], Ting Chen[2], Kerry Kelleher[2], Kiran Khandke[1], Elwira Muszynska[1], Frank Loganzo[1], Edward Rosfjord[1], Judy Lucas[1], Zhengyan Kan[1], Chakrapani Subramanyam[4], Christopher O'Donnell[4], Dario Neri[5], Hans-Peter Gerber[1], Chad May[1], and Puja Sapra[1]

ABSTRACT

Extra domain B splice variant of fibronectin (EDB+FN) is an extracellular matrix protein (ECM) deposited by tumor-associated fibroblasts, and is associated with tumor growth, angiogenesis, and invasion. We hypothesized that EDB+FN is a safe and abundant target for therapeutic intervention with an antibody–drug conjugate (ADC). We describe the generation, pharmacology, mechanism of action, and safety profile of an ADC specific for EDB+FN (EDB-ADC). EDB+FN is broadly expressed in the stroma of pancreatic, non–small cell lung (NSCLC), breast, ovarian, head and neck cancers, whereas restricted in normal tissues. In patient-derived xenograft (PDX), cell-line xenograft (CLX), and mouse syngeneic tumor models, EDB-ADC, conjugated to auristatin Aur0101 through site-specific technology, demonstrated potent antitumor growth inhibition. Increased phospho-histone H3, a pharmacodynamic biomarker of response, was observed in tumor cells distal to the target site of tumor ECM after EDB-ADC treatment. EDB-ADC potentiated infiltration of immune cells, including CD3+ T lymphocytes into the tumor, providing rationale for the combination of EDB-ADC with immune checkpoint therapy. EDB-ADC and anti-PD-L1 combination in a syngeneic breast tumor model led to enhanced antitumor activity with sustained tumor regressions. In nonclinical safety studies in nonhuman primates, EDB-ADC had a well-tolerated safety profile without signs of either on-target toxicity or the off-target effects typically observed with ADCs that are conjugated through conventional conjugation methods. These data highlight the potential for EDB-ADC to specifically target the tumor microenvironment, provide robust therapeutic benefits against multiple tumor types, and enhance activity antitumor in combination with checkpoint blockade.

[1]Pfizer Worldwide Research, Development & Medicine, Oncology Research & Development, Pearl River, New York. [2]Pfizer Worldwide Research, Development & Medicine, BioMedicine Design, Cambridge, Massachusetts. [3]Pfizer Worldwide Research, Development & Medicine, Drug Safety Research & Development, Pearl River, New York. [4]Pfizer Worldwide Medicinal Chemistry, Groton, Connecticut. [5]Institute of Pharmaceutical Sciences, Department of Chemistry and Applied Biosciences, ETH Zurich, Zurich, Switzerland.

Current address for A.T. Hooper, C-P.B. Chang, J. Golas, M. Leal, D. Mathur, and F. Loganzo: Regeneron Pharmaceuticals, Tarrytown, New York; current address for M. Guffroy, Abbvie, North Chicago, Illinois; current address for H. Falahatpisheh, Biosplice Therapeutics, San Diego, California; current address for E. Rosfjord and P. Sapra, AstraZeneca, New York, New York; current address for H P. Gerber, 3T Biosciences, South San Francisco, California; and current address for C. May, Serotiny, South San Francisco, CA.

Corresponding Authors: Kimberly Marquette, BioMedicine Design, Pfizer Inc., 610 Main Street, Cambridge, MA 02139. E-mail: kimberly.marquette@pfizer.com; and Andrea T. Hooper, andrea.hooper@regeneron.com

Introduction

Tumors are no longer defined by only the highly proliferative cancer cell compartment, but instead the diverse repertoire of recruited or locally expanded cells comprising the tumor microenvironment (TME) recognized as active participants and key determinants in cancer progression. The TME, consisting of multiple distinct cell types including fibroblasts, pericytes, blood and lymphatic endothelial cells, innate and adaptive immune cells, as well as growth factors and protease-rich extracellular matrix (ECM), contributes to the stromal compartment orchestrating heterotypic interactions with the cancer cells, progressively driving tumor cell survival, progression, and invasion (1).

Targeted cancer therapeutics, including small molecule inhibitors, monoclonal antibodies (mAbs), and antibody–drug conjugates (ADC), have been largely focused on taking advantage of the cancer cell-related molecular signatures or cell surface proteins to target cancer cells with cytotoxic and other inhibitory agents while minimally affecting normal cells. However, the components of the TME may limit the efficacy of these therapies by driving therapeutic resistance (2). Fibroblasts are the key TME cellular constituents responsible for laying down the ECM components, including the glycoprotein fibronectin. The ECM not only serves as a structural and facilitating scaffold for tumor cell migration via the sequestration and directional concentration of cytokines, but also augments ability of the tumor to withstand harsh conditions such as hypoxia, high metabolic demand, and chemotherapeutic attack (2). Therapies designed to target the TME,

ECM, and stroma to date have had mixed results, and in some cases have been reported to promote worse outcomes (3–6).

Extra domain B (EDB+FN) splice variant of fibronectin 1 consists of a 91 aa domain inserted into fibronectin 1 at the primary transcript level, is a non-internalizing, insoluble, ECM-associated protein, and is a marker of tissue remodeling and angiogenesis (7–11). In solid tumors, EDB+FN is secreted by fibroblasts, myofibroblasts, and vascular smooth muscle cells and is associated with tumor growth, angiogenesis, and invasion (12). Because EDB+FN selectively accumulates in the stroma around new blood vessels in tumors and is largely absent in normal adult vasculature, EDB+FN is a promising target for drug development and tumor-specific delivery of cytotoxic payloads to the TME with an ADC. ADCs employ the exquisite specificity of mAbs for the targeted delivery of highly potent cytotoxic drugs to the tumor site. ADCs have exhibited promising therapeutic results and several products have gained marketing authorization for the treatment of certain malignancies in patients. However, limitations of off-tissue on-target distribution of the antibody into normal tissues remain problematic, thereby limiting the potential for widespread patient benefit. In addition, conventionally conjugated ADCs, where the cytotoxic molecules or payloads are attached to the antibody via lysine side-chain amines or through activated cysteine sulfhydryl groups yielding heterogeneous products with different molar ratios of drug to antibody, may also be limited by the maximum dose that can be administered due to off-target and off-tissue effects of the cytotoxic payload once it dissociates from the antibody.

New classes of ADCs have been developed, which retain potent antitumor activity, but with reduced off-target effects. One example is the site-specific engineered κK183C-K290C antibody conjugated to mcValCitPABC_Aur-06380101 (vc0101), which showed improved linker-payload stability, potent efficacy, and reduced myelosuppression when applied to anti-Her2 trastuzumab (13). The linker-payload vc0101 is completely synthetic and delivers auristatin PF-06380101 (Aur0101), a microtubule depolymerizing agent, also known as a microtubule inhibitor (MTI), with potent anti-mitotic and cytotoxic properties (14, 15). Release of the payload is triggered by proteases such as cathepsins, and both intracellular and extracellular proteases are likely to release the payload (16). The bystander activity of the cell-permeable auristatin payload demonstrates cytotoxicity in a heterogenous tumor environment (13), and we hypothesized would be effective even for an extracellular target such as EDB+FN.

Herein, we show that EDB+FN is an attractive tumor target, as it is broadly expressed and highly enriched in the stromal compartment of multiple cancer types, with a restricted normal tissue expression pattern that is conserved across humans and nonhuman primates. By targeting the stroma and ECM with a novel, highly specific EDB+FN targeting, site-specific ADC, we achieve durable human tumor regressions in mouse models of cancer in a variety of tumor types, harnessing a bystander mechanism without any negative impact on normal tissues. Furthermore, we show that targeting EDB+FN with an ADC induces immune checkpoint mechanisms, as seen by the infiltration of PD-L1 positive immune cells into the tumor parenchyma in a murine breast cancer model. Consequently, a combination benefit is observed with an anti-PD-L1 inhibitor antibody, highlighting the potential to combine EDB-ADC with immune checkpoint inhibitors to enhance clinical benefit. The combination of low-dose EDB-ADC and anti-PD-L1 eliminates tumors. These studies, taken together, expand to non-internalizing ECM, stromal-associated proteins, and proteins involved in mechanisms of angiogenesis, as what we think of as druggable targets for ADCs and other novel tumor tissue targeting modalities.

Materials and Methods

EDB+FN IHC on normal and tumor tissues

Fresh frozen human tumor, normal human tissue, and normal cynomolgous monkey (*Macaca fascicularis*) sections were obtained from the Pfizer Tissue Bank for the assessment of EDB+FN protein expression by immunohistochemistry (IHC). Detailed IHC method information is provided in the Supplementary Materials and Methods.

Construction of anti-EDB+FN antibodies

cDNA encoding a fully human IgG1-Kappa antibody derived from the L19 clone (10) that binds EDB+FN was constructed within a proprietary CHO expression vector using In-Fusion Cloning (Takara Bio). PCR was used to add sequence tags for In-Fusion Cloning to the L19 heavy chain harboring the K(94)R V_H framework mutation (Kabat numbering) to remove a putative glycation liability and the K(290)C (EU numbering or 307 by Kabat numbering) mutation in the constant region to enable site-specific conjugation of vc0101. Similarly, In-Fusion cloning tags were incorporated onto the L19 light chain containing K(183)C (Kabat numbering) within the human Kappa constant region for site-specific conjugation of the linker payload. The heavy chain and light chain were then combined in a single In-Fusion reaction to obtain the final construct within an expression vector for anti-EDB+FN-K(94)R-hIgG1-K290C-Kappa-K(183)C antibody.

A reverse chimeric (rc) antibody comprised of human L19 anti-EDB+FN heavy and light chain variable regions fused to mouse constant regions was generated to produce an ADC for immunocompetent syngeneic tumor models. The cDNA encoding human L19 heavy and light chain variable regions fused to mouse IgG2a and mouse Kappa regions, respectively, were constructed by gene synthesis and subcloned into the pTT5 expression vector (Blue Heron Biotech). Nucleic acid sequence encoding anti-EDB+FN-K(94)R-hIgG1-K290C-Kappa-K(183)C and the rc anti-EDB+FN antibodies was confirmed using double-stranded Sanger DNA sequencing.

Production of anti-EDB+FN antibodies and surface plasmon resonance determination of binding affinity

The anti-EDB+FN-K(94)R-hIgG1-K290C-Kappa-K(183)C antibody expression vector was used to generate stable CHO single-site integration pools and the antibody was purified from the resultant conditioned medium using a two-column purification, Protein A MabSelect SuRe (GE Life Sciences) followed by trimethylaminoethyl (TMAE) at pH 8.1 with weak partitioning to remove high-molecular mass species and process related impurities. Anti-EDB+FN-K(94)R-hIgG1-K290C-Kappa-K(183)C antibody was formulated into PBS-CMF pH 7.2. The rc anti-EDB+FN antibody was produced by transiently co-transfecting HEK-293 cells with expression vectors encoding the heavy and light chains and purified using a two-column purification, Protein A MabSelect SuRe (GE Life Sciences) followed by size-exclusion chromatography (SEC, Superdex 200) and was then formulated into PBS-CMF pH 7.2.

Details and description of the surface plasmon resonance techniques used to evaluate affinity and avidity of the EDB+FN antibodies are provided in the Supplementary Materials and Methods.

Conjugation of EDB to vc0101 and purification of ADCs

Anti-EDB+FN antibodies were conjugated to Aur0101 molecules using mcValCitPABC (ValCit) linker to produce mcValCitPABC_Aur-06380101 (vc0101) ADCs. Anti-EDB+FN antibodies (27.2 mg/mL in PBS, pH 7.2) were reduced with 15-fold molar excess of tris(2-carboxyethyl) phosphine (TCEP) at 37°C for 7 hours, then desalted on

Sephadex-G25 to remove excess TCEP. Interchain disulfide bonds were re-oxidized with 30-fold molar excess of dehydroascorbic acid (DHA) at 4°C overnight, then DHA was removed by desalting. Conjugation was conducted in 9-fold molar excess of mcValCitPAB-C_Aur-06380101 in PBS containing 10% dimethylamine (DMA) at 25°C for 2 hours. Excess linker-payload was quenched with 9-fold excess of L-cysteine at 25°C for 15 minutes, then the ADC dialyzed in PBS at 4°C overnight. The conjugate was purified by SEC on Superose-200 in PBS. The monomer peak was collected, and sample dialyzed into 20 mmol/L histidine/8.5% sucrose, pH 5.8, then sterile filtered and stored at −80°C. Protein concentration was determined via UV spectrophotometry, and the ADC was further characterized via SEC for monomer content (99%–100%), and via LC/MS to measure free drug content (below the level of quantitation) and to calculate the drug–antibody ratio of the resulting EDB-vc0101 (EDB-ADC, DAR = 3.9). Negative control IgG1 antibody (also with κK183C-K290C mutations) was conjugated to the mcValCitPABC_Aur-06380101 and purified under the same conditions as above and generated a product (Neg-vc0101, Neg-ADC) with DAR = 3.9. The rc version of the ADC was conjugated with 2.2-fold molar excess of TCEP and 7-fold excess of mcValCitPABC_Aur-06380101, resulting in an ADC (rcEDB-vc0101, rcEDB-ADC) with DAR of 3.4.

In vitro and *in vivo* pharmacology studies

Experimental conditions for the *in vitro* pharmacology assessments are described in the Supplementary Materials and Methods.

All mouse animal studies were approved by the Pfizer Institutional Animal Care and Use Committee (IACUC) in accordance with the guidelines described in "Guide for the Care and Use of Laboratory Animals" (NRC, 2011). Female NOD.CB17-Prkdcscid (NOD-SCID) mice, athymic nu/nu nude mice, and Balb/c mice 7 to 10 weeks of age (NOD-SCID Stock No.: 394; nu/nu nude, Stock No.: 088; Balb/c Stock No. 028) were obtained from Charles River Laboratories. The human non–small cell lung cancer (NSCLC) patient-derived xenograft (PDX) 37622A1 (PDX-NSX-11122) was subcutaneously passaged *in vivo* as fragments in nu/nu mice as described previously (8). The human pancreatic carcinoma PDX PA0165F/PDX-PAX-13565 (Model Name TM00176) was purchased from The Jackson Laboratory was subcutaneously passaged *in vivo* as fragments in NOD-SCID mice. For studies using NCI-H1975 (H1975, ATCC), athymic nu/nu nude mice were injected subcutaneously in the right flank with 8×10^6 cells suspended in 100% Matrigel (BD Biosciences). For studies using the mouse syngeneic cell line EMT6, 8-week-old Balb/c mice were injected in the left mammary fat pad with 1×10^6 cells suspended in DPBS. For rechallenge experiments in EMT6, once mice had completely eliminated their EMT6 tumors in response to treatment the mice stayed on study tumor-free until Day 40 to 45, then 0.3×10^6 EMT6 cells were re-injected into the right mammary fat pad. Tumors were measured at least twice/week with a Vernier caliper (Mitutoyo) and the tumor volume = (width × width × length)/2. Mice were randomized into study groups when mean tumor volume reached a prespecified tumor volume. Mice were treated intravenously every 4 days with phosphate-buffered saline (PBS; Gibco, Catalog No. 14190–144, as vehicle), Neg-vc0101 (Neg-ADC), EDC-vc0101 (EDB-ADC), or rcEDB-vc0101 (rcEDB-ADC). Mouse IgG2a anti-PD-L1 (reverse chimeric avelumab) was generated in Pfizer.

Histology and IHC for mechanism of action and pharmacodynamic biomarkers

Mechanism of action and pharmacodynamic biomarker studies were conducted in parallel to the efficacy studies. Detailed experimental methods for the IHC studies are available in the Supplementary Material and Methods.

Cynomolgus safety and pharmacokinetic study design

Nonhuman primate studies were approved by Pfizer IACUC, conducted in an Association for Assessment and Accreditation of Laboratory Animal Care–accredited institution, and conducted in accordance with the current guidelines for animal welfare. Experimental conditions for the nonhuman primate studies and pharmacokinetic assessments are available in the Supplementary Materials and Methods.

Data availability

The data generated in this study are available within the article and its supplementary data files.

Results

EDB+FN is broadly expressed in human tumors while restricted in normal tissues

EDB+FN expression in human tumors and normal tissues was studied utilizing a high-sensitivity IHC technique developed to eliminate nonspecific reactivity typical when staining human tissues with a human antibody. Breast cancer ($N = 12$), NSCLC ($N = 15$), ovarian cancer ($N = 12$), head and neck squamous cell cancer ($N = 25$), and pancreatic cancer ($N = 14$) were evaluated for EDB expression (**Fig. 1A**). EDB+FN was expressed in 100% of the tumors stained and expressed at a moderate or high level in the majority of tumors (**Fig. 1A**, inset table). EDB+FN was strongly expressed in the tumor ECM surrounding the tumor parenchymal nests in most tumors (**Fig. 1A**), consistent with previous reports of EDB+FN expression in multiple cancer indications (17–20). There was occasional weaker and less consistent tumor cell staining. EDB+FN IHC on normal human tissues demonstrated the selectivity of the EDB+FN to tumors, with some exceptions such as stromal elements in the muscularis of the gastrointestinal (GI) tract and the ovaries (**Fig. 1B–G**). These findings were consistent with previous reports that EDB+FN is restricted in normal tissues (12). In addition, we examined EDB+FN expression using the TCGA database, showing widespread EDB+FN expression across cancer indications with limited normal tissue expression in tissues either adjacent to tumors (as in the TCGA database) or normal tissues (from GTEX database; Supplementary Fig. S1). Altogether, these data demonstrate EDB+FN is an abundantly expressed tumor ECM protein expressed across a wide breadth of tumor indications with a considerable and favorable tumor to normal (T:N) ratio. This, combined with the restricted normal expression of EDB+FN to predominantly non-proliferating regions, positions EDB+FN as an ideal target for the development of an ADC.

Anti-EDB+FN antibody binding is avidity driven

The binding affinity (K_D) of anti-EDB+FN L19 antibody for human 7-EDB-89 (EDB) was determined to be 231 ± 1.4 nmol/L using a SPR method where the EDB antibody L19 was captured via an anti-human Fc antibody which was directly immobilized onto the biosensor chip and EDB was used as the analyte (Supplementary Table S1). However, when using a different SPR approach, where EDB was directly coupled to the biosensor chip and L19 used as the analyte, the affinity measurement (K_D) was 43.1 ± 6.08 pmol/L—much higher than that determined when EDB was used as the analyte, reflecting a large avidity component (∼5,000-fold) for L19 antibody binding interaction with EDB. Using this latter method, but varying the density of EDB
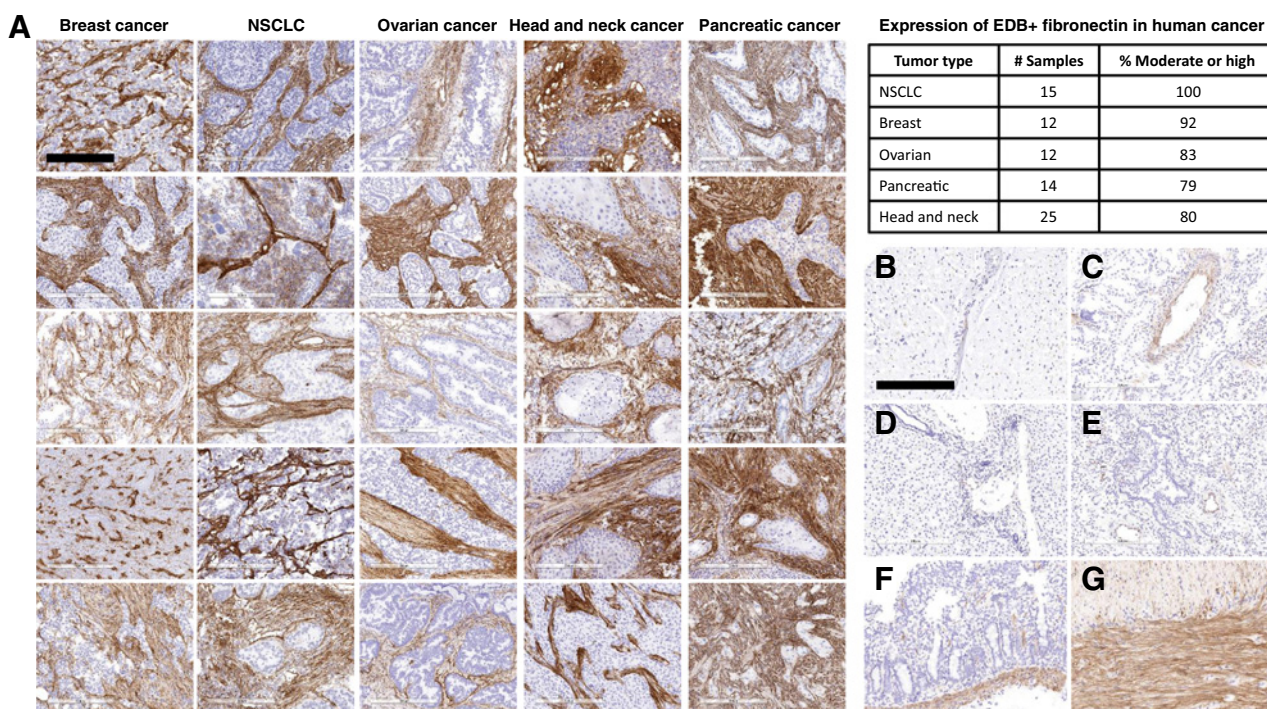
Figure 1.
EDB+FN is expressed in the ECM of multiple tumor types with restricted expression in normal tissues. **A,** Panels of breast cancers, NSCLCs, ovarian cancers, head and neck cancers, and pancreatic cancers were IHC stained for EDB+FN, demonstrating widespread ECM and stromal reactivity in the majority of tumors (inset table). **B–G,** Normal human tissues including heart (**B**), kidney (**C**), liver (**D**), lung (**E**), small intestinal muscularis mucosae (**F**), and muscularis externa (**G**) were stained for EDB+FN. Micron bar = 300 μm.

immobilization, the K_D is proportional to the EDB immobilization levels: 182.5 ± 21.9 or 414.5 ± 201.5 pmol/L using medium or low-density immobilized, respectively, supporting an avidity binding component for L19 antibody interaction with EDB. To eliminate potential biosensor chip matrix effect when EDB is used as the analyte since the pI of recombinant 7-EDB-89 protein is 5.0, EDB was directly immobilized onto the biosensor chip and the antigen binding fragment (Fab) was used as the analyte to remove avidity component. The affinity determined for L19 and L19-K(H94)R-κK(L183)C Fabs binding EDB were 21.3 ± 0.64 and 39.5 ± 7.4 nmol/L, respectively (Supplementary Table S1). The Fab direct binding SPR method offers the most accurate affinity measurement for L19 antibody binding EDB because it eliminates the avidity factor and indicates that the negative charge of biosensor carboxyl matrix may have slowed the on-rates or hastened off-rates due to negative charge of human 7-EDB-89 protein. Collectively, these data suggest that the apparent binding of anti-EDB+FN antibodies is enhanced by significant contribution from avidity when in the presence of high concentrations of antigen or target, which could allow for increased and preferential binding of the anti-EDB+FN antibody or ADC to the tumor microenvironment (where EDB+FN is enriched) versus normal tissues (where EDB+FN is at lower densities or absent)—thereby widening the T:N differential.

EDB-ADC binding to EDB+FN results in cell killing

We hypothesized an ADC is an ideal targeting modality for EDB+FN to further leverage the T:N differential of EDB+FN via the selection of a linker-payload. We employed a linker able to be cleaved by proteases present in the tumor extracellular microenvironment and an MTI payload which is more potent against proliferating cells in the

tumor and less so in normal tissues (21) for the generation of the ADC, together with site-specific conjugation technology which permits exquisite stability of the ADC resulting in reduced off-target toxicities (13).

A site-specific conjugation approach was used to generate EDB-vc0101 (EDB-ADC) with a DAR of 3.9. EDB-ADC binding was assessed via ELISA demonstrating that EDB-ADC bound to 7-EDB-89 with a relative binding measurement of 0.05 nmol/L, which was identical to that of the conventionally conjugated EDB-ADC, suggesting that the ADC has similar binding properties regardless of being a site-specific ADC (Supplementary Table S2). To enable further controlled studies and *in vivo* studies in syngeneic animals, a non-targeted control Neg-ADC was generated (DAR = 3.9) and a reverse chimeric form of the ADC was generated for syngeneic studies (rcEDB-ADC, DAR = 3.4).

Although EDB+FN is predominantly expressed *in vivo* by proliferating or activated fibroblasts and deposited into the extracellular matrix, transformed fibroblastic cell lines such as WI-38 VA-13 provides an opportunity to characterize the cytotoxic potential of ADC candidates *in vitro*. In conjunction, EDB+FN negative cell lines permit testing the specificity of ADCs for their target and to assess the potential for off-target cytotoxic effects. EDB+FN expression was assessed in a panel of cell lines using western blot analysis (Supplementary Fig. S2). Utilizing EDB+FN-positive WI-38 VA-13 fibroblasts, the *in vitro* potency (IC$_{50}$) of EDB-ADC was demonstrated to be 216 ng Ab/mL. This was similar to the *in vitro* potency of the conventionally conjugated EDB-ADC at 185 ng Ab/mL, further demonstrating pharmacologic comparability between the two ADCs. The requirement of EDB+FN for the activity of EDB-ADC was

demonstrated by inclusion of the EDB+FN-negative tumor cell line HT-29, where minimal cytotoxicity was observed similar to Neg-ADC (IC$_{50}$ >10,000 ng Ab/mL), suggesting that the cytotoxicity of EDB-ADC is dependent on EDB+FN expression (Supplementary Fig. S3; Supplementary Table S3).
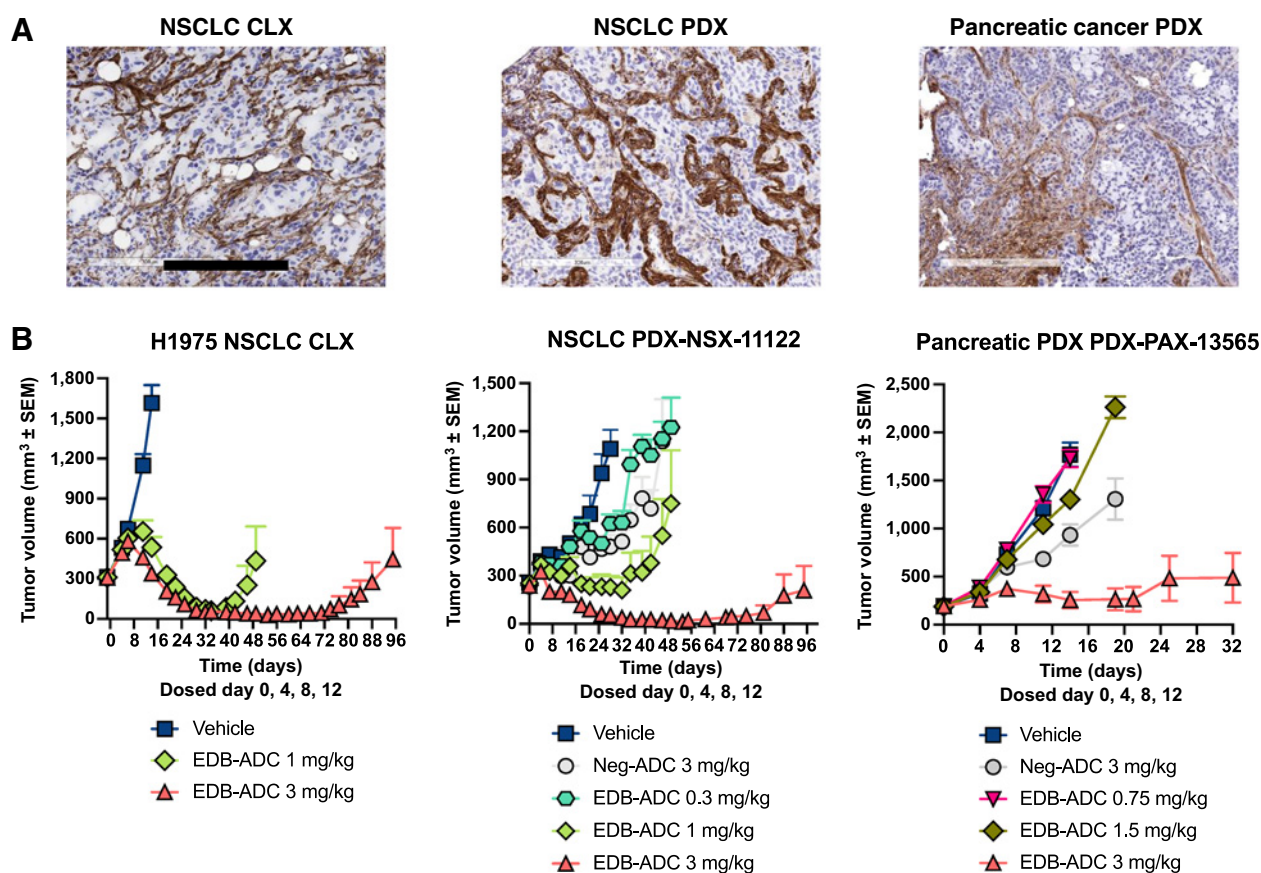
EDB-ADC eliminates human tumors in *in vivo* mouse models of human cancer

EDB+FN expression was evaluated in NSCLC and pancreatic cancer xenografts in immunocompromised mice using IHC. H1975 cell line xenograft (CLX), PDX-NSX-11122, and PDX-PAX-13565 had high EDB+FN protein expression in the tumor stroma (**Fig. 2A**). Utilizing these tumor models, we dosed the mice at staging volume q4dx4 with EDB-ADC intravenously (**Fig. 2B**). In the H1975 model, treatment with EDB-ADC at 1 and 3 mg/kg resulted in a marked decrease in mean tumor volume (MTV) from staging. Tumor growth inhibition (TGI) was statistically significant compared with vehicle-treated mice on the last day the vehicle treated mice were on study (study day 14 ANOVA, $P < 0.0001$). EDB-ADC at 1 and 3 mg/kg resulted in multiple mice with durable complete regressions sustained for 10 to 70 days.

IHC evaluation of human IgG, to detect the antibody component of the ADC, in H1975 tumors 48 hours after a single dose of EDB-ADC, demonstrated that EDB-ADC had widespread distribution through-

out the tumor stroma, similar to the expression of EDB+FN (**Figs. 2A** and **3**). Minimal human IgG was observed in tumors treated with Neg-ADC (**Fig. 3**). Similarly, staining for the ADC payload auristatin showed robust distribution throughout the tumor stroma and ECM in tumors treated with EDB-ADC (**Fig. 3**). Tumors treated with EDB-ADC or Neg-ADC were stained for phospho-histone H3, a marker of mitotic arrest and a pharmacodynamic biomarker of ADC efficacy. Tumors treated with Neg-ADC or EDB-ADC both were positive for phospho-histone H3; however, tumors treated with EDB-ADC had widespread staining of phospho-histone H3+ tumor cells nested within the stromal and ECM pockets where the ADC and payload auristatin were localized (**Fig. 3**), consistent with the greater TGI observed with EDB-ADC compared with Neg-ADC or vehicle control (**Fig. 2B**).

In the NSCLC PDX-NSX-11122 model, treatment with EDB-ADC at 1 and 3 mg/kg resulted in dose-dependent TGI (**Fig. 2B**), with a 18% and 95% decrease in MTV from staging with the 1 and 3 mg/kg dose levels, respectively. TGI for each group was statistically different compared with vehicle treated mice on the last day vehicle treated mice were on study (study day 32 ANOVA, $P < 0.0001$). Eight of 10 mice in the EDB-ADC 3 mg/kg group had complete regressions sustained for 22 to 63 days. Treatment with Neg-ADC did not result in a decrease in MTV in any mice. Treatment of the pancreatic PDX-PAX-13565 model with the EDB-ADC at 3 mg/kg resulted in tumor regressions in 7 of 10 mice. TGI was statistically different

Figure 2.
EDB-ADC eliminates tumors *in vivo* in multiple tumor models. **A,** EDB+FN protein expression by IHC in H1975 CLX, NSCLC PDX, and pancreatic PDX models showing widespread ECM and stromal reactivity mirroring expression in human tumors. **B,** EDB-ADC induces TGI and complete tumor regressions in H1975 CLX, NSCLC PDX, and pancreatic PDX models *in vivo*. Mice bearing indicated human tumors were treated q4dx4 with EDB-ADC or controls at indicated dose levels on Days 0, 4, 8, 12 after tumors reached an average staging volume.
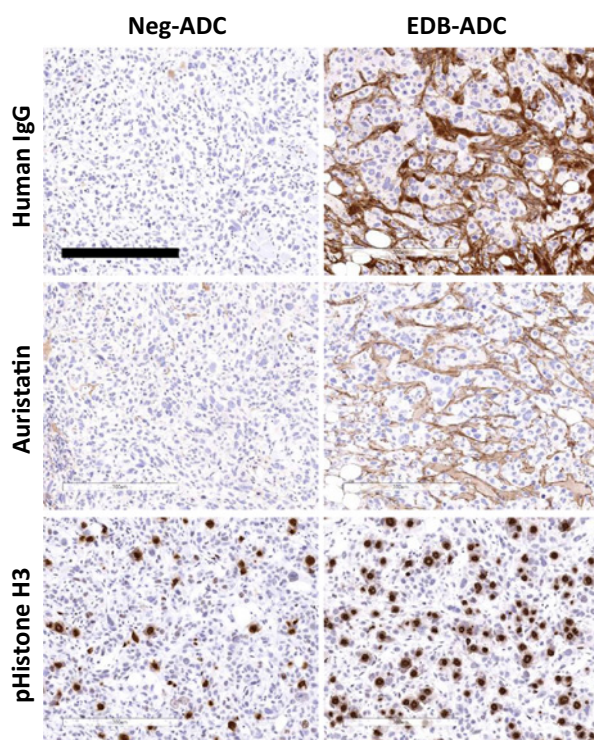
Figure 3.
EDB-ADC localizes to the tumor microenvironment and induces mitotic arrest in tumor cells. Pharmacodynamic IHC to interrogate mechanism of action of EDB-ADC in H1975 tumors 48 hours after a single 3 mg/kg ADC dose, demonstrating ADC distribution (top row as visualized by human IgG antibody IHC) and auristatin payload distribution (middle row, anti-auristatin IHC) in the tumor stromal/ECM compartment, and downstream increase in phospho-histone H3 (pHH3) expression (bottom row). Micron bar = 300 μm.

compared with vehicle treated mice up to last day the vehicle treated mice were on study (study day 7 to 14 ANOVA, $P < 0.0001$). EDB-ADC at 3 mg/kg resulted in 1 of 10 mice with complete regressions. Treatment with Neg-ADC did not result in a decrease in MTV in any mice. Together, we demonstrate that a tumor ECM targeted ADC can result in robust TGI mediated through tumor cell killing likely due to a bystander effect of the cell permeable payload.

EDB-ADC is efficacious in syngeneic mouse tumor model and induces PD-L1 expression and T cell infiltration

EDB+FN was strongly expressed in the syngeneic breast tumor model EMT6 by IHC (**Fig. 4A**). Treatment of EMT6 tumors with a single 9 mg/kg dose of rcEDB-ADC resulted in complete elimination of tumors in all mice. Treatment with 4.5 mg/kg every 4 days twice resulted in elimination of tumors in 7 of 10 mice. Treatment with 3 mg/kg every 4 days three times resulted in TGI and no measurable tumor in 2 mice. Treatment with 1.5 mg/kg every 4 days three times was not statistically different from the vehicle control group (**Fig. 4B**). IHC evaluation of EMT-6 tumors harvested at 48 hours after the second dose of EDB-ADC at 3 mg/kg demonstrated that the tumors treated with EDB-ADC had marked phenotypic alterations of the neoplastic cells. The tumors often had evidence of tumor lysis with a central cavity filled with degenerate dissociated tumor cells and there was marked diffuse immune cell infiltration of mainly lymphocytes but also macrophages with fewer neutrophils (**Fig. 4C**). Although vehicle

treated EMT6 tumors had moderate expression of PD-L1 with modest infiltration of CD3$^+$ T cells, treatment with EDB-ADC significantly increased the expression of PD-L1, both on tumor cells and also on infiltrating macrophages, and increased CD3$^+$ T cells throughout the tumor (**Fig. 4C**, quantified in Supplementary Fig. S4).

## EDB-ADC combines with immunotherapy in syngeneic mouse tumor model

The increased T cell infiltration and upregulation of PD-L1 led us to hypothesize that a combination of EDC-ADC and a checkpoint inhibitor may result in greater TGI at a lower dose of EDB-ADC (**Fig. 5**). Anti-PD-L1 (10 mg/kg dosed i.v. every 3 days three times) resulted in TGI in 2 mice with complete responses that were sustained for 19 days. EDB-ADC 3 mg/kg showed TGI in 9 of 10 mice and complete responses in 6 of 10 mice. Combination of EDB-ADC at 3 mg/kg and anti-PD-L1 resulted complete responses in 9 of 10 mice (**Fig. 5A**). To further examine the potential benefit of EDB-ADC plus checkpoint inhibitor therapy on tumor growth, tumor measurements were evaluated as time for the tumor to increase volume 3-fold from staging size (**Fig. 5B**). Although, anti-PD-L1 had similar median survival compared to vehicle (3.9 days vs. 4.1 days), treatment with EDB-ADC resulted in four tumors with >3-fold increase in tumor volume consistent with previous data showing a suboptimal TGI at this dose. However, EDB-ADC combined with anti-PD-L1 resulted in a single tumor >3-fold from staging volume and was statistically different from both PBS and anti-PD-L1 (log-rank Mantel–Cox $P < 0.0001$). These data demonstrate that combining a stromal or ECM targeting ADC with a checkpoint inhibitor results in effective and durable tumor growth regressions.

To interrogate the advantage of a combination of EDB-ADC with a checkpoint inhibitor, we rechallenged mice that had complete regressions with EMT6 and then assessed the duration for the tumors to regrow (**Fig. 5C**). Mice previously treated with rcEDB-ADC were largely susceptible to tumor challenge [1/6 (17%) remained tumor free]; however, when rcEDB-ADC was combined with anti-PD-L1 5/7 (71%) mice remained tumor free (**Fig. 5C**)—a difference that was statistically significant ($P < 0.05$). These data suggest that there is the added potential for long lasting antitumor immunity when EDB-ADC is combined with a checkpoint inhibitor.

EDB-ADC has a well-tolerated safety profile

As there is 100% protein sequence homology between human and monkey EDB domain (Supplementary Table S4), the cynomolgus monkey is a pharmacologically relevant nonclinical species for toxicity evaluation of EDB-ADC. In addition, L19 antibody demonstrated similar binding affinity to human and monkey EDB in Biacore assay (Supplementary Table S5), and EDB+FN is expressed with a similar pattern of distribution in human and cynomolgous monkey tissues (**Fig. 1B–G**; Supplementary Fig. S5).

EDB-ADC was well tolerated in monkeys up to doses of 12 mg/kg with no indication of target-dependent toxicities in EDB+FN expressing tissues and organs. There were no changes in the general condition of the animals. Clinically relevant toxicities included transient and reversible myelosuppression with associated hematologic changes (marked neutropenia at 12 mg/kg) and corneal findings (minimal to mild increased mitoses/single cell necrosis of epithelial cells with pigment deposition at 12 mg/kg). Additional findings of lesser toxicologic concern included minimally increased mitoses/single cell necrosis of sinusoidal cells in the liver at ≥6 mg/kg. The highest nonseverely toxic dose (HNSTD) of EDB-ADC was considered to be ≥12 mg/kg in the conditions of this study. In general, EDB-ADC-

A

EMT6 syngeneic tumor

B

EMT6 breast carcinoma

C
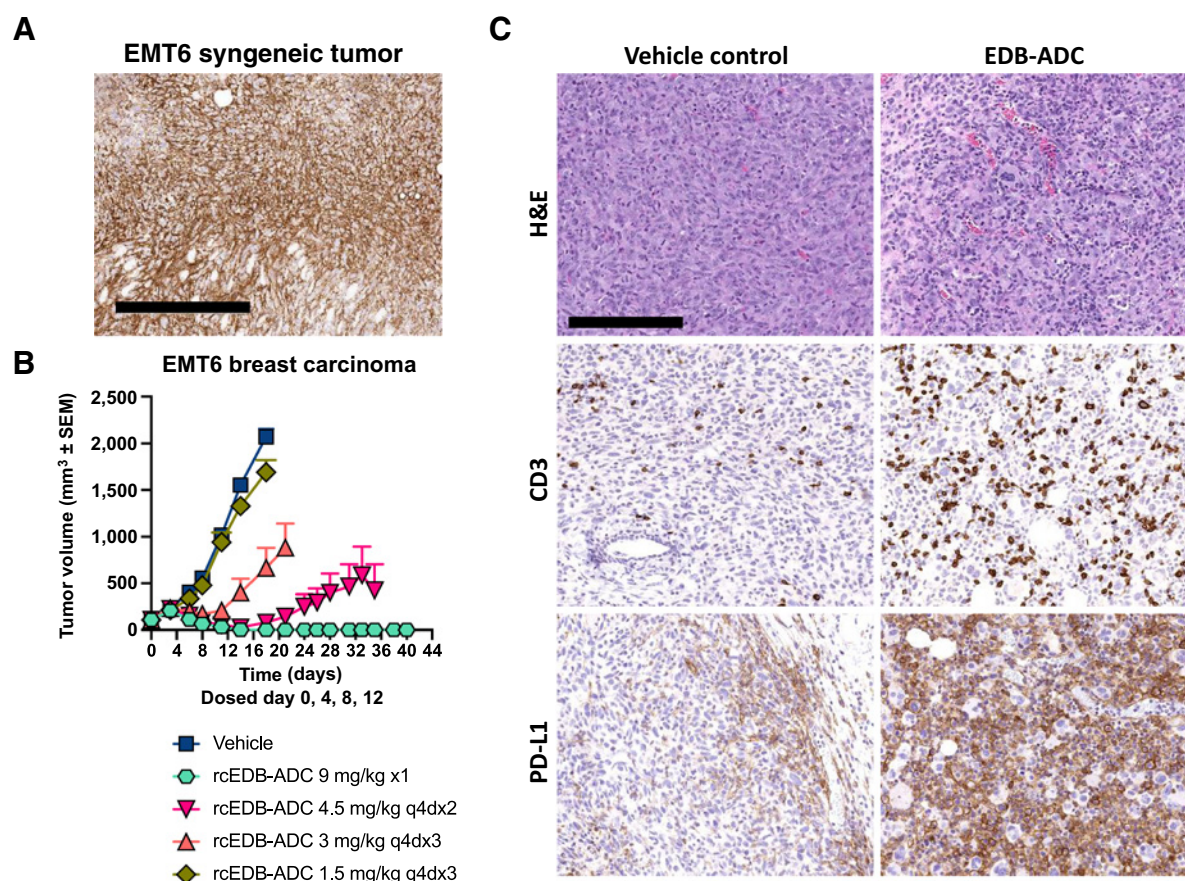
Figure 4.
EDB-ADC eliminates tumors in immunocompetent syngeneic mice & results in increased T cell Infiltration and PD-L1 upregulation. **A,** EDB+FN expression by IHC in EMT6 tumors. **B,** TGI with rcEDB-ADC in EMT6 mice. Mice bearing EMT6 tumors were treated q4d with rcEDB-ADC or vehicle controls at indicated dose levels for 1, 2, or 3 doses as indicated. **C,** EMT6 tumors treated with EDB-ADC were harvested 48 hours after the second dose of 3 mg/kg for pharmacodynamic IHC. H&E staining shows tumor cell lysis and acellular regions (top row), whereas IHC demonstrated increased CD3 infiltration (middle row) and upregulation of PD-L1 (bottom row). Micron bar = 200 μm.

related findings were consistent with target-independent or off-target effects and were similar, though seen here at higher doses, to the toxicity profile reported with other ADCs containing a proteolytically-cleavable linker and MTI payloads. Concentration–time profiles for the ADC and total Ab were similar in all animals as shown by the systemic exposure ratio (ADC/Ab) of approximately 84% (6 mg/kg) and 98% (12 mg/kg), indicative of a stable conjugation process (**Table 2**; Supplementary Fig. S6). In general, the systemic clearance was 0.41 ± 0.06 mL/h/kg and steady-state volume of distribution was 73.1 ± 7.3 mL/kg. Positive anti-drug antibodies (ADA) titers were observed in one of four animals in this study.

In conclusion, EDB-ADC was well tolerated in monkeys without indication of target-dependent toxicities. Importantly, the off-target toxicities, often seen with proteolytically cleavable linkers and MTI payloads (such as bone marrow toxicity and corneal toxicity), appeared to be alleviated by the site-specific conjugation of EDB-ADC.

EDB-ADC has an improved therapeutic index as compared with conventionally conjugated ADC

Therapeutic index (TI) is an index of efficacy used to benchmark and/or compare ADCs. In this case, TI was calculated on the basis of ratio of the average ADC blood concentration (C_{avg}) at the HNSTD

dose in a safety model (cynomolgus monkey) divided by the tumor static concentration (TSC) in an animal model of disease (xenograft human tumor models). A summary of mouse and human pharmacokinetic parameters are shown in **Table 1**. The TI value of EDB-ADC ranged from 4 to 16, depending on which xenograft model was used for the calculation (Supplementary Table S6). This range of TI values (4–16) was higher at the HNSTD of ≥12 mg/kg as compared with the range 2 to 4.9 for a conventionally conjugated EDB-ADC at the monkey HNSTD of ≥5 mg/kg (Supplementary Table S6). Taken together, these data suggest that by using site-specific conjugation the safety margin of an EDB-ADC can be increased due to improved linker-payload stability and reduced myelosuppression without any detriment to antitumor efficacy, thereby giving the potential for a more potent yet better tolerated drug and ultimately an improved TI.

Discussion

We report that EDB+FN is a widely expressed tumor-enriched target for delivery of cytotoxic agents to the extracellular tumor microenvironment with a broad potential for clinical impact. EDB+FN is highly prevalent in multiple tumors, within and across cancer types with high unmet medical need and is restricted in normal
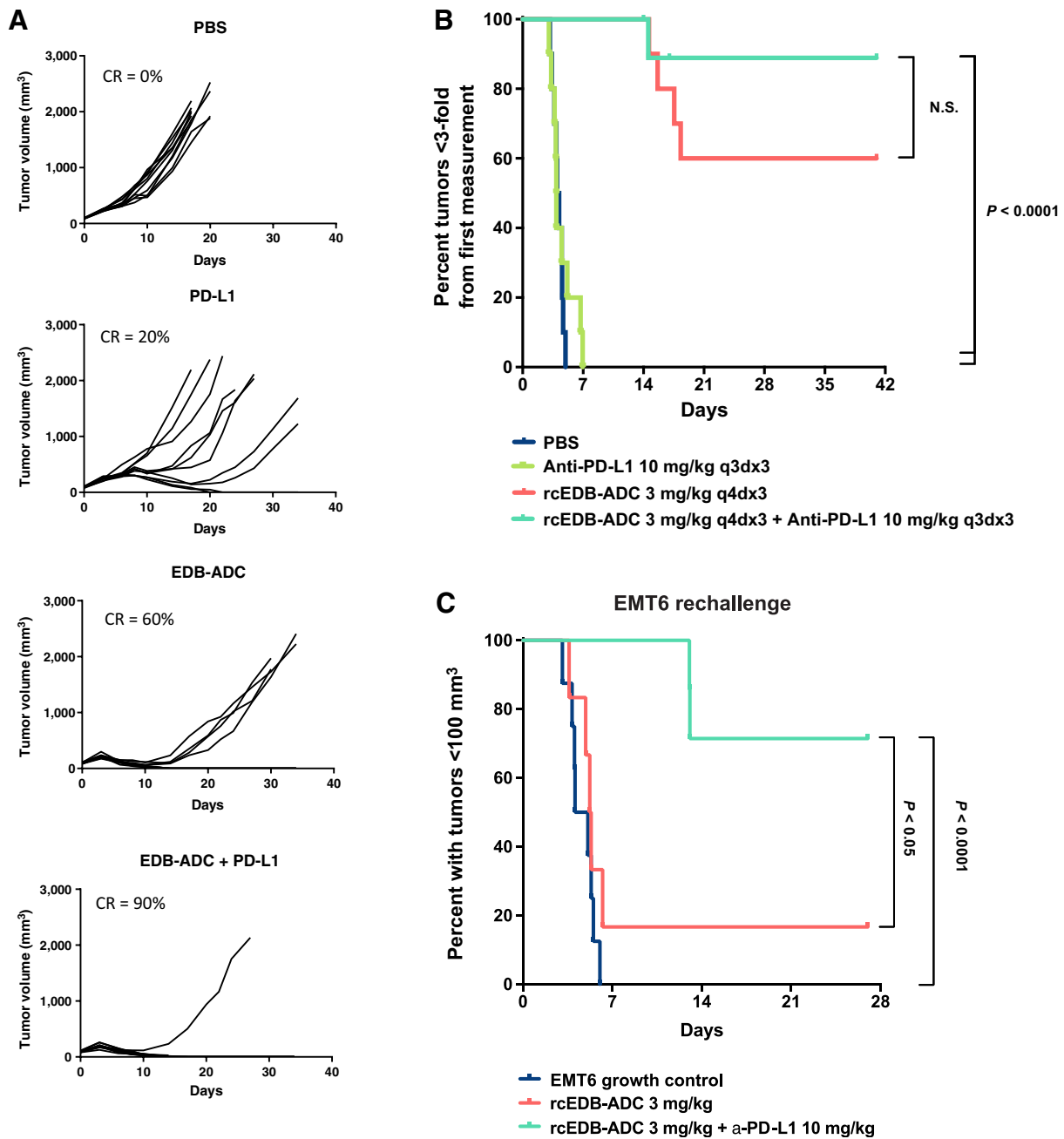
Figure 5.
EDB-ADC demonstrates a combination benefit with checkpoint blockade. **A,** Combination of rcEDB-ADC at 3 mg/kg with anti-PD-L1 10 mg/kg showed a trend towards a combination benefit with 9 of 10 tumors completely regressing as compared with single agents in EMT6 tumor bearing mice. CR = complete regressions. **B**, Kaplan–Meier curves for a time to event analyses in EMT6 tumor bearing mice, showed effectiveness of combining rcEDC-ADC with anti-PD-L1 compared with single agents on % of tumors <3-fold from their first measurement as an indicator of the impact of the combination on tumor growth. **C,** Mice that had complete regressions in the initial study were rechallenged with subcutaneous injection of EMT6 cells and monitored for tumor growth. Mice previously treated with rcEDB-AC plus anti-PD-L1 were resistant to regrowth of new tumors that was significantly different from rcEDB-ADC alone.

tissues. EDB+FN was distributed in the tumor ECM surrounding the tumor parenchyma in all animal models of cancer that were tested and in 100% of human tumors across indications. EDB+FN was at high or moderate levels in the majority of tumors, while restricted in normal tissue, emphasizing the favorable T:N ratio for tumor targeting with an ADC. It is conceivable that because EDB+FN is ECM localized, it may

"bathe" the cells comprising the tumor parenchyma, providing access to previously difficult-to-target cells.

EDB+FN, a non-internalizing ECM target, affords opportunities for intentional therapeutic design to optimize safety and efficacy. Contrary to the assumption that the mechanism of ADCs relies on ADC internalization and intracellular release of the payload, there is

Table 1. Summary of EDB-ADC single-dose pharmacokinetics in mouse and nonhuman primate (NHP, Cynomolgus Monkey).

Model	Dose (mg/kg)	Analyte	C_{max} (μg/mL)	AUC$_{0-tau}$ (μg*h/mL)	Terminal $t_{1/2}$ (day)	ADC/Ab (%)
Mouse	3	Ab	59.6	3,820	4.0	90
		ADC	62.4	3,450	3.4	
NHP	6	Ab	159	,16250	6.6	84
		ADC	148	13,700	5.9	
		Payload	0.00012	0.034	NA	NA
	12	Ab	258	24,800	6.1	98
		ADC	268	24,450	5.8	
		Payload	0.00046	0.096	NA	NA

Note: Mouse tau = 336 hours; NHP tau = 504 hours.
Abbreviations: Ab, antibody; NA, not applicable.

growing evidence that non-internalizing ADCs can demonstrate antitumor efficacy (22), elegantly demonstrated by the work of Neri and colleagues showing the preclinical efficacy of non-internalizing ADCs targeting the ECM targets EDA+FN and Tenascin C (16, 22–24). We hypothesized using an ADC to target EDB+FN would result in the extracellular release of the cytotoxic payload, resulting in bystander killing of tumor cells—mechanistically distinct from other clinical stage ADCs, which target membrane internalizing proteins. Herewith, we describe the first non-internalizing ADC targeted against EDB+FN for which the therapeutic profile was optimized via bioengineering based on biological features of the target and tumor microenvironment in categories such as antibody avidity versus affinity, linker selection for extracellular release, payload selection for proliferating cells, and site-specific conjugation for stability.

Although standard practice is often to select mAb candidates with low nmol/L affinity for their target, these high-affinity antibodies may result in off-tissue on-target binding and potential for toxicity. To avoid this pitfall and capitalize on the T:N ratio of EDB+FN, we selected an antibody for the EDB-ADC that is of moderate affinity but demonstrates high avidity. The anti-EDB+FN antibody binds to EDB+FN in an avidity driven manner, and antibody binding is enhanced in the presence of higher concentrations of target. On the basis of these data, we propose a model that high enrichment of EDB+FN in the tumor microenvironment compared with normal tissue allows for avidity-driven binding, preferentially in the TME, thereby in effect widening the T:N differential.

EDB+FN is expressed at the invasive, high remodeling regions of a tumor where extracellular proteases (such as cathepsins) involved in invasion and tumor remodeling are enriched. On the other hand, healthy homeostatic quiescent normal tissues do not have large reservoirs of proteases in the extracellular tissue microenvironment. Therefore, by utilization of the ValCit linker, which requires proteolytic cleavage for release of the payload and resulting cytotoxic activity, we capitalized on enriched expression of EDB+FN at sites of tumor remodeling, simultaneously high in protease activity, to further bias the activity of the ADC towards the tumor. We propose this is a self-amplifying cyclical mechanism—when cells die there is release of additional proteases into the TME, resulting in cleavage of the linker, releasing more payload, and subsequent further cell killing. In addition, we selected a potent antimitotic MTI auristatin Aur0101 as the cytotoxic payload for EDB-ADC. Aur0101 results in cell-cycle arrest and apoptosis of target cells, mechanistically limiting the cytotoxic activity to those cells which are actively dividing (14, 15), thereby

deliberately biasing ADC activity to proliferating tumor cells as opposed to those non-proliferative cells within the normal tissues.

The success of ADCs in the clinic has been hindered by the inability to "dose up" to reach greater plasma exposure permitting maximal antitumor effects due to off-target ADC activity as a consequence of off-tissue release of the payload, resulting in dose-limiting toxicities as have been seen with MTI ADCs such as neutropenia (25). Although ADCs using Aur0101 as a payload have progressed into the clinic (26), because conventional conjugation methodologies were employed this left the potential to be capped by the highest dose that can be safely administered. To address this potential liability, we used site-specific conjugation of the MTI to cysteine K183C and K290C residues. Importantly, there was no significant toxicity observed with the EDB-ADC in nonhuman primates, whereas the in vivo efficacy studies in preclinical experimental tumor models of human cancer demonstrated that the site-specific EDB-ADC retains activity in a dose- and antibody-dependent fashion. Site-specific conjugation of EDB-ADC increased the safety margin as an effect of improved linker-payload stability, leading to a reduction in off-target myelosuppression without any detriment to antitumor efficacy. Utilizing a site-specific conjugate against a target with restricted normal tissue expression such as EDB+FN leads us to anticipate being able to dose higher in humans providing greater potential for antitumor efficacy. As the TI was improved with the site-specific EDB-ADC as compared with the conventionally conjugated ADC, it is reasonable to hypothesize that in clinical studies an increased plasma exposure may be attainable due to the unique combination of the site-specific ADC and the highly tumor selective ECM antigen as the target.

Taken together, by maximizing features of the EDB-ADC through bioengineering and molecular design focused on the ECM target, optimized affinity/avidity, linker and payload selection, and site-specific technology, we developed an ADC with the potential for widespread clinical utility across human cancers along with an improved TI and potential for diverse mechanisms of action as compared with currently available ADCs. On the basis of the data presented herein, the mechanisms of antitumor efficacy with EDB-ADC may include cell death/cell-cycle arrest of tumor cells and immunomodulation. Indeed, we showed that EDB-ADC enabled checkpoint blockade as the combination of EDB-ADC and anti-PD-L1 resulted in long-lived tumor regressions. Additional mechanisms such as death or modulation of fibroblastic stromal cells, de-regulated angiogenesis or cytotoxic vascular targeting/collapse, vascular normalization, induction of cellular differentiation, and/or impediment of the epithelial-to-mesenchymal transition remain plausible but need further study. In addition, as splice variants of FN1 have been published to be increased in patients who have received prior chemotherapy, and splice variants of FN1 are reported to be involved in chemo- and radio-resistance (27, 28), further investigations can be pursued to combine EDB-ADC with standards of care (SOC) such as chemotherapy and radiotherapy either through sequential or simultaneous administration.

The studies presented herein demonstrate potent, tumor selective cytotoxicity with a well-tolerated safety profile using a cytotoxic ADC targeting EDB+FN, warranting further investigation of EDB-ADC in the clinic. Our data definitively support the concept of safe and efficacious targeting ADCs to non-internalizing antigens, such as extracellular matrix and stromal proteins, thereby expanding the scope of antigens that can be targeted using this modality for the treatment of cancer. Although this work highlights the successful delivery of cytotoxic payloads to the TME by targeting EDB+FN, the concept of a non-internalizing ADC could potentially be extended to deliver a

variety of other payloads, such as immunomodulators that reprogram the tumor stroma and immune repertoire to enhance therapeutic responses in patients.

Authors' Disclosures

Authors' Contributions

A.T. Hooper: Conceptualization, data curation, formal analysis, supervision, visualization, methodology, writing–original draft, project administration, writing–review and editing. K. Marquette: Conceptualization, formal analysis, supervision, visualization, methodology, writing–original draft, project administration, writing–review and editing. C.B. Chang: Conceptualization, data curation, formal analysis, visualization, methodology, writing–review and editing. J. Golas: Conceptualization, data curation, formal analysis, supervision, visualization, methodology, writing–original draft, writing--review and editing. S. Jain: Data curation, methodology, writing–original draft. M. Lam: Data curation, formal analysis, methodology, writing–review and editing. M. Guffroy: Conceptualization, data curation, formal analysis, visualization, writing–original draft, writing–review and editing. M. Leal: Conceptualization, data curation, formal analysis, supervision, visualization, methodology, writing–original draft, project administration, writing–review and editing. H. Falahatpisheh: Conceptualization, data curation, formal analysis, visualization, methodology. D. Mathur: Conceptualization, data curation, supervision, visualization, writing–original draft, writing–review and editing. T. Chen: Data curation, formal analysis, methodology, writing–review and editing. K. Kelleher: Data curation, formal analysis, methodology, writing–review and editing. K. Khandke: Conceptualization, data curation, formal analysis, supervision, methodology, writing–review and editing. E. Muszynska: Methodology, writing–review and editing. F. Loganzo: Conceptualization, data curation, formal analysis, supervision, visualization, methodology, writing–original draft, project administration, writing–review and editing. E. Rosfjord: Data curation, formal analysis, supervision, visualization, methodology, writing–original draft, writing–review and editing. J. Lucas: Conceptualization, data curation, formal analysis, supervision, methodology, writing–review and editing. Z. Kan: Conceptualization, formal analysis, visualization, methodology, writing–review and editing. C. Subramanyam: Conceptualization, data curation, supervision, methodology, writing–review and editing. C. O'Donnell: Conceptualization, supervision, project administration, writing–review and editing. D. Neri: Conceptualization, writing–review and editing. H. Gerber: Conceptualization, formal analysis, supervision, writing–review and editing. C. May: Conceptualization, data curation, formal analysis, supervision, visualization, methodology, writing–review and editing. P. Sapra: Conceptualization, formal analysis, supervision, writing–original draft, writing–review and editing.

Acknowledgments

Note

References

1. Hanahan D, Weinberg RA. Hallmarks of cancer: the next generation. Cell 2011; 144:646–74.
2. Huelsken J, Hanahan D. A subset of cancer-associated fibroblasts determines therapy resistance. Cell 2018;172:643–4.
3. Valkenburg KC, de Groot AE, Pienta KJ. Targeting the tumour stroma to improve cancer therapy. Nat Rev Clin Oncol 2018;15:366–81.
4. Ozdemir BC, Pentcheva-Hoang T, Carstens JL, Zheng X, Wu CC, Simpson TR, et al. Depletion of carcinoma-associated fibroblasts and fibrosis induces immunosuppression and accelerates pancreas cancer with reduced survival. Cancer Cell 2014;25:719–34.
5. Rhim AD, Oberstein PE, Thomas DH, Mirek ET, Palermo CF, Sastra SA, et al. Stromal elements act to restrain, rather than support, pancreatic ductal adenocarcinoma. Cancer Cell 2014;25:735–47.
6. Lee JJ, Perera RM, Wang H, Wu DC, Liu XS, Han S, et al. Stromal response to Hedgehog signaling restrains pancreatic cancer progression. Proc Natl Acad Sci U S A 2014;111:E3091–100.
7. Carnemolla B, Balza E, Siri A, Zardi L, Nicotra MR, Bigotti A, et al. A tumor-associated fibronectin isoform generated by alternative splicing of messenger RNA precursors. J Cell Biol 1989;108:1139–48.
8. Carnemolla B, Leprini A, Querze G, Urbini S, Zardi L. Novel self-association fibronectin sites. Biochem Cell Biol 1996;74:745–8.
9. Castellani P, Borsi L, Carnemolla B, Biro A, Dorcaratto A, Viale GL, et al. Differentiation between high- and low-grade astrocytoma using a human recombinant antibody to the extra domain-B of fibronectin. Am J Pathol 2002;161:1695–700.
10. Gutman A, Kornblihtt AR. Identification of a third region of cell-specific alternative splicing in human fibronectin mRNA. Proc Natl Acad Sci U S A 1987;84:7179–82.
11. Zardi L, Carnemolla B, Siri A, Petersen TE, Paolella G, Sebastio G, et al. Transformed human cells produce a new fibronectin isoform by preferential alternative splicing of a previously unobserved exon. EMBO J 1987; 6:2337–42.

12. Menrad A, Menssen HD. ED-B fibronectin as a target for antibody-based cancer treatments. Expert Opin Ther Targets 2005;9:491–500.

13. Graziani EI, Sung M, Ma D, Narayanan B, Marquette K, Puthenveetil S, et al. PF-06804103, a site-specific anti-HER2 antibody-drug conjugate for the treatment of HER2-expressing breast, gastric, and lung cancers. Mol Cancer Ther 2020;19: 2068–78.

14. Damelin M, Bankovich A, Bernstein J, Lucas J, Chen L, Williams S, et al. A PTK7-targeted antibody-drug conjugate reduces tumor-initiating cells and induces sustained tumor regressions. Sci Transl Med 2017;9: eaag2611.

15. Maderna A, Doroski M, Subramanyam C, Porte A, Leverett CA, Vetelino BC, et al. Discovery of cytotoxic dolastatin 10 analogues with N-terminal modifications. J Med Chem 2014;57:10527–43.

16. Gebleux R, Stringhini M, Casanova R, Soltermann A, Neri D. Non-internalizing antibody-drug conjugates display potent anti-cancer activity upon proteolytic release of monomethyl auristatin E in the subendothelial extracellular matrix. Int J Cancer 2017;140:1670–9.

17. Birchler MT, Milisavlijevic D, Pfaltz M, Neri D, Odermatt B, Schmid S, et al. Expression of the extra domain B of fibronectin, a marker of angiogenesis, in head and neck tumors. Laryngoscope 2003;113:1231–7.

18. Kaczmarek J, Castellani P, Nicolo G, Spina B, Allemanni G, Zardi L. Distribution of oncofetal fibronectin isoforms in normal, hyperplastic and neoplastic human breast tissues. Int J Cancer 1994;59:11–6.

19. Ohnishi T, Hiraga S, Izumoto S, Matsumura H, Kanemura Y, Arita N, et al. Role of fibronectin-stimulated tumor cell migration in glioma invasion in vivo: clinical significance of fibronectin and fibronectin receptor expressed in human glioma tissues. Clin Exp Metastasis 1998;16:729–41.

20. Schwager K, Villa A, Rosli C, Neri D, Rosli-Khabas M, Moser G. A comparative immunofluorescence analysis of three clinical-stage antibodies in head and neck cancer. Head Neck Oncol 2011;3:25.

21. Sapra P, Damelin M, Dijoseph J, Marquette K, Geles KG, Golas J, et al. Long-term tumor regression induced by an antibody-drug conjugate that targets 5T4, an onco-fetal antigen expressed on tumor-initiating cells. Mol Cancer Ther 2013;12:38–47.

22. Dal Corso A, Cazzamalli S, Gebleux R, Mattarella M, Neri D. Protease-cleavable linkers modulate the anticancer activity of noninternalizing antibody-drug conjugates. Bioconjug Chem 2017;28:1826–33.

23. Perrino E, Steiner M, Krall N, Bernardes GJ, Pretto F, Casi G, et al. Curative properties of noninternalizing antibody–drug conjugates based on maytansinoids. Cancer Res 2014;74:2569–78.

24. Dal Corso A, Gebleux R, Murer P, Soltermann A, Neri D. A non-internalizing antibody-drug conjugate based on an anthracycline payload displays potent therapeutic activity in vivo. J Control Release 2017;264:211–8.

25. Donaghy H. Effects of antibody, drug and linker on the preclinical and clinical toxicities of antibody-drug conjugates. MAbs 2016;8:659–71.

26. Rosen LS, Wesolowski R, Baffa R, Liao KH, Hua SY, Gibson BL, et al. A phase I, dose-escalation study of PF-06650808, an anti-Notch3 antibody-drug conjugate, in patients with breast cancer and other advanced solid tumors. Invest New Drugs 2020;38:120–30.

27. Ou J, Pan F, Geng P, Wei X, Xie G, Deng J, et al. Silencing fibronectin extra domain A enhances radiosensitivity in nasopharyngeal carcinomas involving an FAK/Akt/JNK pathway. Int J Radiat Oncol Biol Phys 2012;82:e685–91.

28. Ou J, Deng J, Wei X, Xie G, Zhou R, Yu L, et al. Fibronectin extra domain A (EDA) sustains CD133(+)/CD44(+) subpopulation of colorectal cancer cells. Stem Cell Res 2013;11:820–33.